NANO LETTERS

Letter

pubs.acs.org/NanoLett

Controlled Synthesis of Nitrogen-Doped Graphene on Ruthenium from Azafullerene

Xiangmin Fei,[†,‡] Joshua Neilson,[†] Yanbang Li,[§] Vanessa Lopez,[†] Simon J. Garrett,[∥] Liangbing Gan,[§] Hong-Jun Gao,[‡] and Li Gao*[,†]

[†]Department of Physics and Astronomy, California State University, Northridge, California 91330, United States

[‡]Institute of Physics, Chinese Academy of Sciences, Beijing 100190, China

[§]Key Laboratory of Bioorganic Chemistry and Molecular Engineering of the Ministry of Education, College of Chemistry and Molecular Engineering, Peking University, Beijing 100871, China

[∥]Department of Chemistry and Biochemistry, California State University, Northridge, California 91330, United States

S *Supporting Information*

ABSTRACT: The controlled synthesis of high-quality nitrogen (N) doped single layer graphene on the Ru(0001) surface has been achieved using the N-containing sole precursor azafullerene ($C_{59}NH$). The synthesis process and doping properties have been investigated on the atomic scale by combining scanning tunneling microscopy and X-ray photoelectron spectroscopy measurements. We find for the first time that the concentration of N-related defects on the N-doped graphene/Ru(0001) surface is tunable by adjusting the dosage of sole precursor and the number of growth cycles. Two primary types of N-related defects have been observed. The predominant bonding configuration of N atoms in the obtained graphene layer is pyridinic N. Our findings indicate that the synthesis from heteroatom-containing sole precursors is a very promising approach for the preparation of doped graphene materials with controlled doping properties.

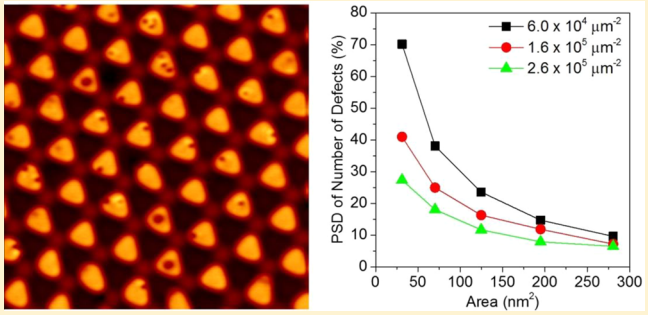

KEYWORDS: *Nitrogen-doped graphene, nitrogen-containing sole precursor, scanning tunneling microscopy, doping properties, azafullerene*

Graphene, a single atomic layer of sp^2-hybridized carbon atoms arranged into a hexagonal honeycomb lattice, is the first discovered truly two-dimensional crystalline material and has attracted intense interest due to its exotic properties.[1,2] Substitutional doping of graphene with heteroatoms is one of the most fascinating strategies for tailoring various properties of graphene and hence expanding the practical applications of this wonder material.[3,4] Nitrogen is one of the most appealing dopant elements for graphene because N-doped graphene materials have wide potential applications in field-effect transistors, fuel cells, solar cells, lithium ion batteries, supercapacitors, sensors, photocatalysis, and gas storage.[3−8] In order to promote the practical applications of N-doped graphene materials, it is of utmost importance to achieve their synthesis with a high level of control over doping properties because different applications require different doping properties. N-doped graphene materials have been synthesized by several different approaches,[3−5] among which the synthesis from N-containing sole precursors has recently demonstrated its feasibility with several different sole precursors.[8−13] The N-containing sole precursors contain both C and N atoms in one molecule. This synthesis approach offers three potential advantages. First, compared to the synthesis using two separate precursors, one for C and the other for N, this approach can substantially simplify the synthesis process. Second, doping properties can potentially be well controlled by choosing different precursors, metal catalysts, and synthesis parameters. Third, high doping homogeneity can potentially be achieved more easily compared to other approaches because both N and C atoms are from the same precursor. The synthesis of N-containing precursors is currently an active research direction in synthetic chemistry, which has been expanding and will continue to expand the library of available precursors for this synthesis approach.

The capability to control the doping properties is one of the most important criteria for evaluating different synthesis approaches. However, for the synthesis from N-containing sole precursors, it remains largely unexplored how to tune the doping concentration using the same sole precursor, and the investigation of doping homogeneity is still lacking. In addition, the bonding configuration of N atoms in the graphene lattice is strongly dependent on synthesis approaches and experimental

Received: January 4, 2017
Revised: March 30, 2017
Published: April 11, 2017

DOI: 10.1021/acs.nanolett.7b00038
Nano Lett. 2017, 17, 2887−2894

conditions.[3,5,8,9,14−19] However, for the synthesis from N-containing sole precursors, experimental investigations so far are still limited in terms of sole precursors, metal catalysts, and other experimental parameters.[8−13] Therefore, it is highly desirable to explore new and effective sole precursors, different metal catalysts, and other various experimental parameters in order to achieve a higher level of control over the bonding configurations of N atoms in graphene.

Here we report the controlled synthesis of high-quality N-doped single layer graphene from a new N-containing sole precursor, that is, azafullerene ($C_{59}NH$), on the Ru(0001) surface. Fullerene and graphene are two allotropes of carbon. To the best of our knowledge, this is the first study on the transformation of heterofullerene into heteroatom-doped graphene. The synthesis process and doping properties are investigated by combining scanning tunneling microscopy (STM) and X-ray photoelectron spectroscopy (XPS) measurements. STM measurements provide atomic-scale insights into the synthesis process, the structural quality of doped graphene layer, and the doping properties. XPS measurements provide information about the bonding configurations of N atoms in the graphene layer. For the first time, we find that the concentration of N-related defects in the graphene layer can be tuned by adjusting the dosage of sole precursor and the number of growth cycles. The spatial homogeneity of N-related defects is high and improves with increasing doping concentration. The percentage standard deviation (PSD) of the number of doping defects is lower than 10% for 150 nm^2 and larger areas when the concentration of doping defects is 2.6×10^5 μm^{-2}. XPS measurements indicate that the predominant doping configuration produced by this synthesis approach is pyridinic N, while some N atoms are in an anionic state due to their bonding with the Ru surface. High-resolution STM measurements have been corroborated with XPS results and suggest that the pyridinic N doping configuration is correlated to single-atom vacancies in the graphene layer.

All the synthesis experiments and STM measurements were performed using a Unisoku ultrahigh vacuum (UHV) low-temperature STM system (USM1500S) with a base pressure lower than 2×10^{-10} Torr. The single crystal Ru(0001) surface (Princeton Scientific) was cleaned by repeated cycles of Ar^+ ion sputtering (1.5 keV, 1×10^{-5} Torr, 30 min), annealing at ~1500 K for 10 min, and subsequent flash annealing to ~1680 K. The $C_{59}NH$ molecules were prepared following the procedures reported by Xin et al.[20] and were thoroughly degassed in UHV prior to molecular deposition. The deposition of $C_{59}NH$ molecules was performed by thermal evaporation at ~600 K from an Al_2O_3 crucible. The Ru(0001) substrate was held at room temperature during molecular deposition. The synthesis of N-doped graphene was performed by annealing the $C_{59}NH$/Ru(0001) sample from room temperature up to 900 °C with a step of 100 °C and a dwell time of 5 min at each temperature step. All of the STM measurements were carried out at 77 K with tungsten tips prepared by electrochemical etching. XPS measurements were performed using a Physical Electronics PHI 5200 XPS system with an Al Kα X-ray source (1486.6 eV) and hemispherical analyzer with a pass energy of 44.7 eV. The instrument was calibrated by using sputter cleaned Au ($4f_{7/2}$ = 84.0 ± 0.1 eV binding energy) and Cu ($2p_{3/2}$ = 932.7 ± 0.1 eV binding energy) foils.

The structure of the N-containing precursor $C_{59}NH$ is shown in the inset of Figure 1a. In each $C_{59}NH$ molecule, one C atom

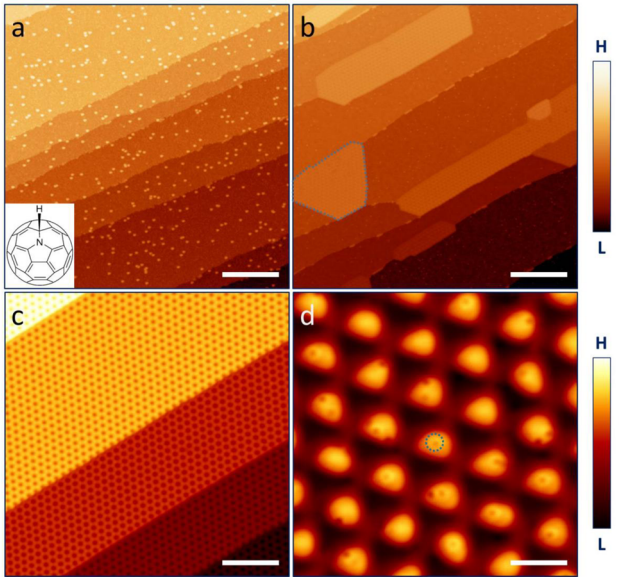

Figure 1. (a) STM image of the Ru(0001) surface after deposition of 0.01 ML $C_{59}NH$ molecules. (b) STM image of graphene patches formed by annealing 0.01 ML $C_{59}NH$ molecules on Ru(0001) to 900 °C. One of the graphene islands is highlighted by the dashed blue line. (c) STM image of a full monolayer of graphene synthesized from the precursor $C_{59}NH$. (d) STM image showing the N-related defects (dark spots) in the synthesized graphene layer on Ru(0001). One of the N-related defects is highlighted by the dashed blue circle. Scanning parameters: (a) V_{bias} = +3 V, I = 5 pA; (b) V_{bias} = +3 V, I = 5 pA; (c) V_{bias} = +3 V, I = 5 pA; and (d) V_{bias} = +500 mV, I = 50 pA. Scale bars: (a) 40 nm; (b) 40 nm; (c) 20 nm; (d) 3 nm.

of the fullerene cage structure is replaced by one N atom.[20−22] Figure 1a is a representative STM image of the Ru(0001) surface after room-temperature deposition of 0.01 monolayer (ML) $C_{59}NH$ molecules. The molecules adsorb on the Ru surface as isolated molecules. After annealing this $C_{59}NH$/Ru(0001) sample up to 900 °C, $C_{59}NH$ molecules transformed into graphene patches, as shown in Figure 1b. This transformation suggests that the $C_{59}NH$/Ru is a strongly interacting interface, similar to the C_{60}/Ru, C_{60}/Ni, C_{60}/Pt, and C_{60}/Ir interfaces.[23−27] The transformation of $C_{59}NH$ precursor molecules into graphene starts at around 500 °C and the high-quality graphene layer can be obtained at around 900 °C, as shown by a series of annealing experiments at different temperatures and subsequent STM measurements (see Supporting Information Figure S1). A full monolayer of graphene can be obtained after repeated cycles of $C_{59}NH$ deposition and subsequent annealing, as shown in Figure 1c. Similar to previous efforts on the synthesis of graphene on the Ru(0001) surface,[28,29] the high-quality single layer graphene has also been achieved on the Ru(0001) surface using the sole precursor $C_{59}NH$ in our experiments, as indicated by the highly ordered moiré pattern in Figure 1c. More importantly, close-up STM images show a number of dark spots distributed over the moiré pattern, as shown in Figure 1d. The dark spots are much more apparent in the bright regions than in the rest of the moiré pattern. The concentration values of dark spots reported in this paper were calculated by counting the dark spots only in the bright regions, which might lead to an underestimate by a factor of 5.6 (see Supporting Information Note 1). The optimal range of bias voltage is between +0.5 and +2.0 V for clearly imaging all these dark spots simultaneously. These dark spots

DOI: 10.1021/acs.nanolett.7b00038
Nano Lett. 2017, 17, 2887−2894

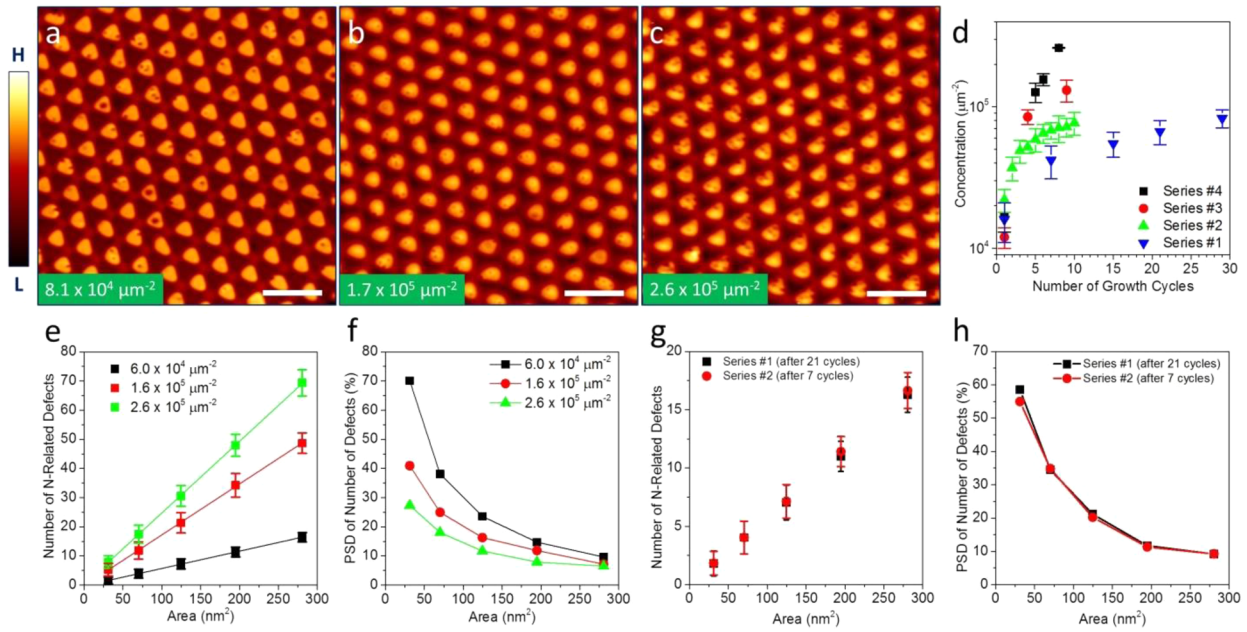

Figure 2. (a–c) STM images of synthesized N-doped graphene on Ru(0001) with three different concentrations of N-related defects: (a) 8.1×10^4 μm^{-2}; (b) 1.7×10^5 μm^{-2}; (c) 2.6×10^5 μm^{-2}. Scanning parameters: (a) V_{bias} = +1 V, I = 50 pA; (b) V_{bias} = +500 mV, I = 50 pA; and (c) V_{bias} = +2 V, I = 50 pA. Scale bars for (a–c): 6 nm. (d) Concentration of N-related defects as a function of growth cycles for four series of growth experiments. The error bars are standard deviations of concentration measured in different regions. The precursor dosages during each growth cycle for Series #1–4 are 0.01, 0.11, 0.23, and 0.37 ML, respectively. (e) Number of N-related defects as a function of surface area for three samples with different concentrations. The error bars are standard deviations of number of N-related defects measured in different regions. The straight lines are linear fits of the data. (f) PSD of the number of N-related defects as a function of surface area for the three samples in (e). (g,h) Comparison of spatial homogeneity of N-related defects between two samples with the same defect concentration (6.8×10^4 μm^{-2}) but from two different series of growth experiments. (g) Number of N-related defects as a function of surface area. The error bars are standard deviations of number of N-related defects measured in different regions. (h) PSD of the number of N-related defects as a function of surface area.

were observed all over the graphene/Ru(0001) surface obtained by annealing the $C_{59}NH$/Ru(0001) surface but were not observed in pristine graphene layers on Ru(0001) obtained by varied approaches including annealing the C_{60}/Ru(0001) surface.[24] These dark spots are unlikely related to the impurities in the $C_{59}NH$ sample (see Supporting Information Note 2). In addition, the content of N dopants measured by XPS is consistent with the concentration of dark spots measured by STM, as discussed below. Therefore, the observed dark spots can be assigned as N-related defects on the graphene/Ru(0001) surface. It is worth noting that the STM images of boron doped single layer graphene on Ru(0001) show similar dark spots, which have been associated with B dopants in the graphene lattice.[30]

On the basis of the number ratio of N and C atoms in the precursor $C_{59}NH$ (N/C = 1:59), the concentration of N atoms in the synthesized graphene layer would be ~6.4×10^5 μm^{-2} if all N and C atoms from the precursor remain on the Ru surface during annealing and form the N-doped graphene layer. However, our experiments show that the concentration of N-related defects after one growth cycle is in the range from 1.0×10^4 μm^{-2} to 3.0×10^4 μm^{-2}, which is much lower than 6.4×10^5 μm^{-2}. Three factors may contribute to this apparent difference. First, some N and C atoms from the precursor desorbed from the Ru surface when the precursor molecules decomposed into intermediate small species at the elevated temperature, which has been validated by comparing the coverage of precursor $C_{59}NH$ molecules before annealing with the coverage of graphene after annealing; therefore, if the percentage of desorption is higher for N atoms than for C atoms, the number ratio of N and C atoms in the obtained graphene layer should be lower than the ratio in the precursor $C_{59}NH$ molecule. Second, the formation energies for all doping configurations of N atoms in graphene are higher than the formation energy for pristine graphene,[14,31] which may also contribute to this apparent difference. Third, some of the N-related defects on STM images might be induced by multiple N atoms for each defect. Despite the relatively low concentration of N-related defects after the first growth cycle, it is very encouraging to find that the concentration of N-related defects can be well tuned by adjusting the dosage of sole precursor and the number of growth cycles. Here one growth cycle includes the dosing of sole precursor at room temperature and subsequent annealing to 900 °C.

Figure 2a–c shows typical STM images of obtained N-doped single layer graphene on the Ru(0001) surface with three different concentrations of N-related defects. Figure 2d shows how the concentration of N-related defects evolves with the number of growth cycles in four series of growth experiments. The four series correspond to four different dosages of sole precursor during each growth cycle, that is, 0.01, 0.11, 0.23, and 0.37 ML, for Series #1–4, respectively. In each series, the concentration of N-related defects increases with increasing number of growth cycles, and the increase is faster if the dosage of sole precursor is higher during each growth cycle. With a precursor dosage of 0.01 ML, the concentration increases from 1.6×10^4 μm^{-2} for 1 growth cycle up to 8.3×10^4 μm^{-2} for 29 growth cycles; in contrast, with a higher precursor dosage of 0.37 ML, the concentration increases from 1.7×10^4 μm^{-2} for 1 growth cycle up to 2.6×10^5 μm^{-2} for 8 growth cycles. During

DOI: 10.1021/acs.nanolett.7b00038
Nano Lett. 2017, 17, 2887–2894

each growth cycle, the sole precursor $C_{59}NH$ molecules decompose into intermediate small species at the elevated temperature. The intermediate species diffuse and aggregate into the graphene lattice, leading to the increase of graphene coverage; meanwhile, the N-containing intermediate species act as the N source, diffusing along the existing graphene surface and leading to the doping of more N atoms into the graphene layer. When the coverage of graphene increases with more growth cycles, the bare Ru surface area decreases accordingly (see Supporting Information Figure S2). $C_{59}NH$ molecules decompose on the bare Ru surface but not on the graphene surface at elevated temperature (see Supporting Information Figure S3). With increasing growth cycles, less and less $C_{59}NH$ molecules can decompose during one cycle due to the decreasing of the bare Ru surface area, although the dosage of $C_{59}NH$ molecules for each cycle remains the same in one series. That explains our observation that in each series the concentration of N-related defects tends to saturate with increasing growth cycles, as shown in Figure 2d. Although the synthesis of N-doped graphene from N-containing sole precursors has been reported recently,[8−13] this is the first time a feasible and efficient strategy for tuning the doping concentration of N has been discovered while using the same sole precursor.

The spatial homogeneity of N-related defects can be characterized by STM measurements. By counting the number of defects in different regions (see Supporting Information Note 3), we have plotted the number of N-related defects as a function of surface area, as shown in Figure 2e. Three samples with different defect concentrations are included in Figure 2e. The straight solid lines are linear fits of the data. It is clear that the number of N-related defects increases linearly with the surface area. The slopes of the linear fits are the concentrations. The spatial homogeneity of N-related defects can be quantitatively evaluated by the PSD of the number of defects. The PSD is the ratio of standard deviation to mean. The calculations of PSD were performed using the data in Figure 2e. Our results show that the PSD decreases with increasing surface area, as shown in Figure 2f. For all three different concentrations, PSD values lower than 10% can be achieved for 280 nm^2 and larger areas. In addition, the homogeneity of spatial distribution improves with increasing defect concentration, and the PSD values are lower than 10% for 150 nm^2 and larger areas when the defect concentration is 2.6×10^5 μm^{-2}. Figure 2d indicates that the same concentration of defects can be achieved from different series of growth experiments. For example, a defect concentration of 6.8×10^4 μm^{-2} can be achieved by either 21 cycles of growth in Series #1 or 7 cycles of growth in Series #2, as shown in Figure 2d. STM images of the 2 samples (21 cycles in Series #1 and 7 cycles in Series #2) are shown in Supporting Information Figure S4. The statistics shown in Figure 2g,h, that is, the number of N-related defects as a function of surface area and the PSD of the number of N-related defects as a function of surface area, indicate that the spatial homogeneity of N-related defects is roughly the same for the two samples.

The existence of N atoms in the synthesized graphene layer is confirmed by XPS measurements, and the predominant bonding configuration of N atoms in the graphene lattice has been identified based on the binding energy (BE) positions of N peaks. Figure 3 shows the XPS spectra measured for the synthesized N-doped single layer graphene on the Ru(0001) surface. The concentration of N-related defects on this sample,

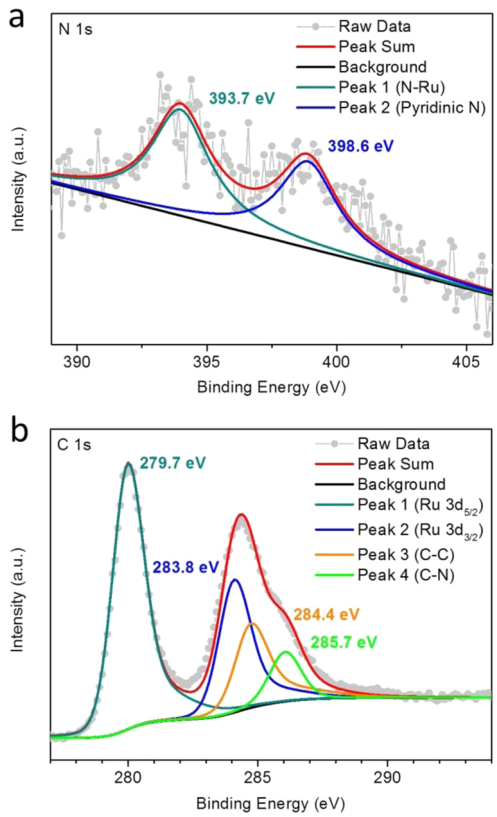

Figure 3. XPS of the N-doped graphene layer on Ru(0001). (a) N 1s spectra. (b) C 1s spectra.

as determined by STM measurements, is around 8.3×10^4 μm^{-2}. Previous studies have shown that there are three common doping configurations for N in graphene, that is, pyridinic N, pyrrolic N, and graphitic N. The specific bonding configurations of N in graphene can be identified by analyzing the N 1s XPS spectrum. The binding energies of N 1s electrons range from 394 eV BE (N^{3-}) to 408 eV BE (N^{5+}) depending on chemical environment. The N 1s spectrum can be deconvoluted into several individual peaks corresponding to different bonding configurations.[8,32−35] The N 1s spectrum in Figure 3a can be deconvoluted into two different peaks with binding energies of 393.7 and 398.6 eV, respectively. Previous studies have shown that the N 1s binding energy is around 394 eV if N is in an anionic state, which usually corresponds to the bonding between N and metal atoms such as Ti.[36] Therefore, the peak at 393.7 eV BE in Figure 3a can be attributed to the N atoms that are trapped beneath the graphene layer and bound to Ru. Previous studies have also shown that the peak positions are at 398.1−399.3 eV BE for pyridinic N, 399.8−401.2 eV BE for pyrrolic N, and 400.0−402.7 eV BE for graphitic N, respectively.[5,8,37,38] Therefore, the peak at 398.6 eV BE in Figure 3a can be attributed to pyridinic N doping configuration. XPS results suggest that the predominant bonding configuration of N atoms in the obtained graphene layer is pyridinic N, which originates from sp^2 hybridized N atoms bonded with two sp^2 hybridized C atoms at the edges or defects of the graphene lattice. The pyridinic N doping configuration is always accompanied by defects or edges in the graphene layer. The content of N with the other doping configurations is below the detection limit of XPS. As discussed above, the XPS results confirm that N atoms have been successfully incorporated into

DOI: 10.1021/acs.nanolett.7b00038
Nano Lett. 2017, 17, 2887−2894

the graphene lattice. The C 1s XPS spectrum, as shown in Figure 3b, can be deconvoluted into four different peaks centered at 279.7, 283.8, 284.4, and 285.7 eV BE, respectively. These first two peaks can be assigned to Ru $3d_{5/2}$, Ru $3d_{3/2}$, respectively. The peak centered at 284.4 eV BE can be assigned to sp^2 hybridized C atoms in graphene.[28,39,40] The peak centered at 285.7 eV BE can be assigned to sp^2 hybridized C atoms bonded with N.[5,14,18,35,41,42] The content of N in graphene is around 1.8%, as determined from the C 1s peaks centered at 284.4 and 285.7 eV as well as the N 1s peak centered at 398.6 eV, which is in good agreement with the concentration of dark spots observed in STM measurements (see Supporting Information Note 4). In addition, XPS measurements of two different samples show that the areas of N 1s peaks increase with increasing concentration of dark spots, which also suggests that the dark spots are related to N (see Supporting Information Figure S5).

To gain further atomic-scale insights into the bonding configuration of N atoms in the obtained doped graphene layer, high-resolution STM measurements of the N-related defects have been performed. Figure 4a,b shows bias-dependent STM

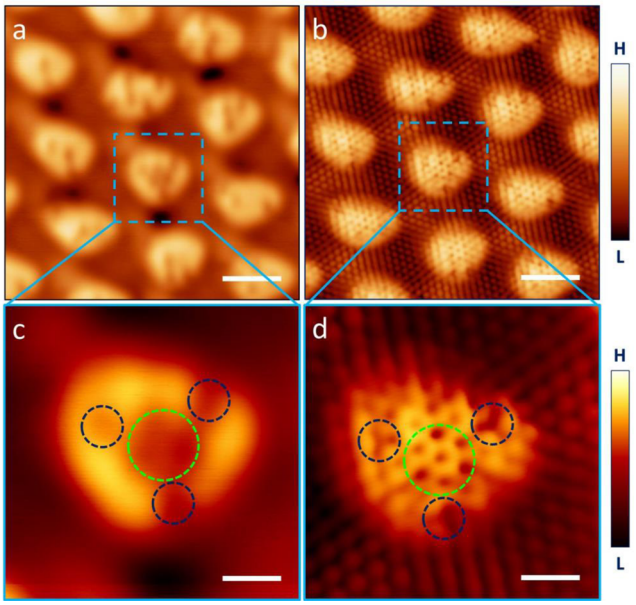

Figure 4. (a,b) Bias-dependent STM images of N-doped graphene on Ru(0001) synthesized from $C_{59}NH$. The two light blue dashed squares enclose the same atop region of the moiré pattern. (c,d) Close-up STM images of the marked regions in (a,b), respectively. The N-related defects marked by green dashed circles are not accompanied by vacancies in graphene, while the defects marked by dark blue dashed circles are accompanied by single-atom vacancies in graphene. Scanning parameters: (a) V_{bias} = +1 V, I = 50 pA; (b) V_{bias} = +10 mV, I = 5 nA; (c) V_{bias} = +1 V, I = 50 pA; and (d) V_{bias} = +10 mV, I = 5 nA. Scale bars: (a) 2; (b) 2; (c) 0.6; and (d) 0.6 nm.

images of the same region on the N-doped graphene/Ru(0001) surface, which were recorded at +1 V and +10 mV, respectively. The concentration of N-related defects on this sample is around $2.6 \times 10^5\ \mu m^{-2}$. It is interesting to note that the number of defects observed at +10 mV with atomic resolution is evidently less than that observed at +1 V. The dashed squares on these two images indicate the same region and the corresponding close-up STM images are shown in Figure 4c,d. It is clear that the graphene lattice of the defects marked by the green dashed circle still exhibits the hexagonal honeycomb structure; however, the graphene lattice of the defects marked by the dark blue dashed circles exhibit single-atom vacancies. Therefore, some defects on the sample surface are accompanied by vacancies in graphene, while the other defects have the hexagonal honeycomb structure. Our extensive STM measurements indicate that the defects with single-atom vacancies account for (49.8 ± 3.1)% of all the defects on the sample surface.

In order to clearly image individual defects, further high-resolution STM measurements were performed on an N-doped graphene/Ru(0001) surface with a lower defect concentration, as shown in Figure 5. Our extensive measurements reveal that

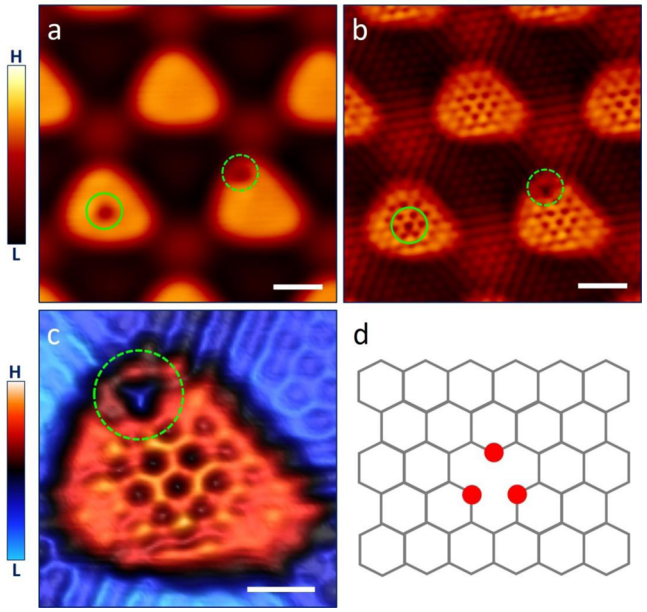

Figure 5. Two primary types of N-related defects observed in STM measurements. (a,b) Bias-dependent STM images of one area on the N-doped graphene/Ru(0001) surface. (c) High-resolution STM image of the defect marked by the dashed green circles in (a,b). (d) Sketch of the pyridinic N_3V_1 doping configuration. Scanning parameters: (a) V_{bias} = +1 V, I = 50 pA; (b) V_{bias} = +10 mV, I = 1 nA; (c) V_{bias} = +10 mV, I = 1 nA. Scale bars: (a) 1; (b) 1; (c) 0.5 nm.

there are primarily two types of N-related defects. For the first type of defects, such as the defects marked by the green solid circle in Figure 5a,b, the atomic-resolution STM images of such defects are the same as the one of pristine graphene. Navarro et al. recently found that the oxygen atoms trapped between the graphene layer and Ru substrate also lead to dark spots on corresponding STM images.[43] More importantly, our XPS measurements have indicated the existence of N atoms trapped beneath the graphene layer and bound to Ru, as discussed above. Therefore, this first type of defects can be attributed to the N atoms that are trapped between the graphene layer and Ru substrate. For the second type of defects, such as the defects marked by the green dashed circle in Figure 5a–c, the atomic-resolution STM images of such defects exhibit a single-atom vacancy in the graphene lattice, as shown in Figure 5b,c. We propose that such single-atom vacancies are decorated with N atoms due to three reasons. First, such single-atom vacancies were rarely observed in the undoped graphene layer on Ru(0001) because pure vacancies in graphene are energetically unfavorable.[44,45] Second, the decoration with N atoms can

DOI: 10.1021/acs.nanolett.7b00038
Nano Lett. 2017, 17, 2887–2894

stabilize vacancies in graphene and the formation energies of N-decorated vacancies are much lower compared to pure vacancies.[31,44] Third, XPS measurements indicate that pyridinic N, which is always accompanied by vacancies, is the predominant doping configuration; and, in the meanwhile, the single-atom vacancies shown in Figures 4d and 5b,c are the predominant type of vacancy in the obtained N-doped graphene layer. These N-decorated single-atom vacancies have a regular triangular geometry. Ab initio density functional theory (DFT) calculations have been carried out to determine the formation energies of various bonding configurations of N atoms in the graphene lattice.[14,31,44] Pyridinic N_3V_1, that is, one single-atom vacancy decorated with three N atoms, as sketched in Figure 5d, has been theoretically identified as one of the most energetically favorable doping configurations and, in the meanwhile, it is the only configuration exhibiting a regular triangular geometry with a single-atom vacancy.[14,31,44] Therefore, this second type of defects is most likely correlated to pyridinic N_3V_1 doping configuration. It is worth mentioning that the same doping configuration, that is, one single-atom vacancy decorated with three heteroatoms, has also been observed in oxygen-doped graphene experimentally by Guo et al. using high-resolution scanning transmission electron microscopy.[46] Besides the above two primary types of defects that were detected by both STM and XPS, there exists a third type of defects (See Supporting Information Figure S6) that accounts for only a small portion of all defects on the sample surface and was observed only by STM. It is worth mentioning that the electron scattering[47] induced by doping defects was observed in STM measurements of N-doped single layer graphene on the SiO_2,[14] Cu,[13,15] SiC,[48,49] and graphene/SiC[16] surfaces. However, such electron scattering was not observed in our STM measurements of N-doped single layer graphene on Ru(0001), which can be ascribed to the disturbance induced by the strong interfacial interaction between graphene and Ru.[50−52]

It is noted that previous ab initio DFT calculations have predicted that the graphitic N_1 configuration has the lowest formation energy among all possible doping configurations for N-doped graphene.[14,31,44] However, experimental efforts have shown that the predominant doping configurations in N-doped graphene vary with different synthesis approaches and experimental parameters.[3,5,8,9,14−19] In fact, pyridinic N doped graphene was also obtained on the Cu surface using acetonitrile or pyridine as the sole precursor.[8,9] Our efforts reported here reveal a new and effective strategy for preparing high-quality pyridinic N doped graphene with high doping homogeneity and tunable doping concentration.

In summary, we have achieved the controlled synthesis of high-quality N-doped single layer graphene on the Ru(0001) surface using the sole precursor $C_{59}NH$. For the first time, we find that the concentration of N-related defects can be precisely tuned by adjusting the dosage of sole precursor and the number of growth cycles. High-resolution STM and XPS measurements reveal that the predominant doping configuration is pyridinic N with a single-atom vacancy in the obtained graphene layer. This work provides crucial atomic-scale insights into the synthesis process and doping properties for the synthesis of N-doped graphene from N-containing sole precursors, which will boost the controlled synthesis of graphene materials doped with various heteroatoms from diverse heteroatom-containing sole precursors.

■ ASSOCIATED CONTENT

Supporting Information

The Supporting Information is available free of charge on the ACS Publications website at DOI: 10.1021/acs.nanolett.7b00038.

STM images obtained after annealing a sample of 1.57 ML $C_{59}NH$ on Ru(0001) to different temperatures. The area percentage of bright regions of the moiré pattern on the graphene/Ru surface. Purity of the $C_{59}NH$ sample. Coverage of graphene and concentration of N-related defects as a function of growth cycles. Different behaviors of azafullerene molecules on Ru and graphene surfaces during deposition and annealing processes. Sizes of surface regions used for concentration statistics. STM images of two samples with the same defect concentration but from two different series of growth experiments. Comparison between the pyridinic N content measured by XPS and the defect concentration measured by STM. XPS N 1s spectra for two samples with different concentrations of dark spots. Bias-dependent STM images of a third type of defects (PDF)

■ AUTHOR INFORMATION

Corresponding Author

*Phone: 818-677-4365. Fax: 818-677-3234. E-mail: li.gao@csun.edu.

ORCID

Liangbing Gan: 0000-0001-6646-3452

Li Gao: 0000-0001-6615-6807

Notes

The authors declare no competing financial interest.

■ ACKNOWLEDGMENTS

We gratefully acknowledge the financial supports from California State University Northridge, National Science Foundation (NSF) under Grant DMR-1205734, and National Natural Science Foundation of China (Grant 21132007). We also acknowledge the Molecular Instrumentation Center at University of California Los Angeles for the use of characterization facilities.

■ ABBREVIATIONS

N, nitrogen; C, carbon; Ru, ruthenium; STM, scanning tunneling microscopy; XPS, X-ray photoelectron spectroscopy; PSD, percentage standard deviation; UHV, ultrahigh vacuum; ML, monolayer; BE, binding energy; DFT, density functional theory; SiO_2, silicon dioxide; SiC, silicon carbide

■ REFERENCES

(1) Novoselov, K. S.; Geim, A. K.; Morozov, S. V.; Jiang, D.; Zhang, Y.; Dubonos, S. V.; Grigorieva, I. V.; Firsov, A. A. Electric Field Effect in Atomically Thin Carbon Films. *Science* **2004**, *306*, 666−669.

(2) Geim, A. K.; Novoselov, K. S. The Rise of Graphene. *Nat. Mater.* **2007**, *6*, 183−191.

(3) Wang, X. W.; Sun, G. Z.; Routh, P.; Kim, D.-H.; Huang, W.; Chen, P. Heteroatom-Doped Graphene Materials: Syntheses, Properties and Applications. *Chem. Soc. Rev.* **2014**, *43*, 7067−7098.

(4) Narita, A.; Wang, X. Y.; Feng, X. L.; Müllen, K. New Advances in Nanographene Chemistry. *Chem. Soc. Rev.* **2015**, *44*, 6616−6643.

(5) Wang, H. B.; Maiyalagan, T.; Wang, X. Review on Recent Progress in Nitrogen-Doped Graphene: Synthesis, Characterization, and Its Potential Applications. *ACS Catal.* **2012**, *2*, 781−794.

DOI: 10.1021/acs.nanolett.7b00038
Nano Lett. 2017, 17, 2887−2894

(6) Ito, Y.; Christodoulou, C.; Nardi, M. V.; Koch, N.; Kläui, M.; Sachdev, H.; Müllen, K. Tuning the Magnetic Properties of Carbon by Nitrogen Doping of Its Graphene Domains. *J. Am. Chem. Soc.* **2015**, *137*, 7678−7685.
(7) Shan, J. Q.; Liu, Y. X.; Liu, P.; Huang, Y. S.; Su, Y. Z.; Wu, D. Q.; Feng, X. L. Nitrogen-Doped Carbon-Encapsulated SnO_2-SnS/Graphene Sheets with Improved Anodic Performance in Lithium Ion Batteries. *J. Mater. Chem. A* **2015**, *3*, 24148−24154.
(8) Reddy, A. L. M.; Srivastava, A.; Gowda, S. R.; Gullapalli, H.; Dubey, M.; Ajayan, P. M. Synthesis of Nitrogen-Doped Graphene Films For Lithium Battery Application. *ACS Nano* **2010**, *4*, 6337−6342.
(9) Jin, Z.; Yao, J.; Kittrell, C.; Tour, J. M. Large-Scale Growth and Characterizations of Nitrogen-Doped Monolayer Graphene Sheets. *ACS Nano* **2011**, *5*, 4112−4117.
(10) Cui, T. X.; Lv, R. T.; Huang, Z. H.; Zhu, H. W.; Kang, F. Y.; Wang, K. L.; Wu, D. H. Effect of Feed Rate on the Production of Nitrogen-Doped Graphene from Liquid Acetonitrile. *Carbon* **2012**, *50*, 3659−3665.
(11) Ito, Y.; Christodoulou, C.; Nardi, M. V.; Koch, N.; Sachdev, H.; Müllen, K. Chemical Vapor Deposition of N-Doped Graphene and Carbon Films: The Role of Precursors and Gas Phase. *ACS Nano* **2014**, *8*, 3337−3346.
(12) Zhang, Y.; Zhang, Y. F.; Li, G.; Lu, J. C.; Lin, X.; Du, S. X.; Berger, R.; Feng, X. L.; Müllen, K.; Gao, H.-J. Direct Visualization of Atomically Precise Nitrogen-Doped Graphene Nanoribbons. *Appl. Phys. Lett.* **2014**, *105*, 023101.
(13) Zabet-Khosousi, A.; Zhao, L. Y.; Pálová, L.; Hybertsen, M. S.; Reichman, D. R.; Pasupathy, A. N.; Flynn, G. W. Segregation of Sublattice Domains in Nitrogen-Doped Graphene. *J. Am. Chem. Soc.* **2014**, *136*, 1391−1397.
(14) Lv, R. T.; Li, Q.; Botello-Mendez, A. R.; Hayashi, T.; Wang, B.; Berkdemir, A.; Hao, Q. Z.; Elias, A. L.; Cruz-Silva, R.; Gutierrez, H. R.; et al. Nitrogen-Doped Graphene: Beyond Single Substitution and Enhanced Molecular Sensing. *Sci. Rep.* **2012**, *2*, 586.
(15) Zhao, L. Y.; He, R.; Rim, K. T.; Schiros, T.; Kim, K. S.; Zhou, H.; Gutierrez, C.; Chockalingam, S. P.; Arguello, C. J.; Palova, L.; et al. Visualizing Individual Nitrogen Dopants in Monolayer Graphene. *Science* **2011**, *333*, 999−1003.
(16) Deng, D. H.; Pan, X. L.; Yu, L.; Cui, Y.; Jiang, Y. P.; Qi, J.; Li, W.-X.; Fu, Q.; Ma, X. C.; Xue, Q. K.; et al. Toward N-Doped Graphene via Solvothermal Synthesis. *Chem. Mater.* **2011**, *23*, 1188−1193.
(17) Lai, L. F.; Potts, J. R.; Zhan, D.; Wang, L.; Poh, C. K.; Tang, C. H.; Gong, H.; Shen, Z. X.; Lin, J. Y.; Ruoff, R. S. Exploration of the Active Center Structure of Nitrogen-Doped Graphene-Based Catalysts for Oxygen Reduction Reaction. *Energy Environ. Sci.* **2012**, *5*, 7936−7942.
(18) Wei, D. C.; Liu, Y. Q.; Wang, Y.; Zhang, H. L.; Huang, L. P.; Yu, G. Synthesis of N-Doped Graphene by Chemical Vapor Deposition and Its Electrical Properties. *Nano Lett.* **2009**, *9*, 1752−1758.
(19) Qu, L. T.; Liu, Y.; Baek, J.-B.; Dai, L. M. Nitrogen-Doped Graphene as Efficient Metal-Free Electrocatalyst for Oxygen Reduction in Fuel Cells. *ACS Nano* **2010**, *4*, 1321−1326.
(20) Xin, N. N.; Huang, H.; Zhang, J. X.; Dai, Z. F.; Gan, L. B. Fullerene Doping: Preparation of Azafullerene $C_{59}NH$ and Oxafulleroids $C_{59}O_3$ and $C_{60}O_4$. *Angew. Chem., Int. Ed.* **2012**, *51*, 6163−6166.
(21) Vostrowsky, O.; Hirsch, A. Heterofullerenes. *Chem. Rev.* **2006**, *106*, 5191−5207.
(22) Hummelen, J. C.; Bellavia-Lund, C.; Wudl, F. Heterofullerenes. *Top. Curr. Chem.* **1999**, *199*, 93−134.
(23) Cepek, C.; Goldoni, A.; Modesti, S. Chemisorption and Fragmentation of C_{60} on Pt(111) and Ni(110). *Phys. Rev. B: Condens. Matter Mater. Phys.* **1996**, *53*, 7466−7472.
(24) Lu, J.; Yeo, P. S. E.; Gan, C. K.; Wu, P.; Loh, K. P. Transforming C_{60} Molecules into Graphene Quantum Dots. *Nat. Nanotechnol.* **2011**, *6*, 247−252.
(25) Perdigão, L. M. A.; Sabki, S. N.; Garfitt, J. M.; Capiod, P.; Beton, P. H. Graphene Formation by Decomposition of C_{60}. *J. Phys. Chem. C* **2011**, *115*, 7472−7476.
(26) Yamada, Y.; Yamada, S.; Nakayama, T.; Sasaki, M.; Tsuru, T. Electronic Modificaiton of C_{60} Monolayers via Metal Substrates. *J. J. Appl. Phys.* **2011**, *50*, 08LB06.
(27) Fei, X. M.; Zhang, X.; Lopez, V.; Lu, G.; Gao, H. J.; Gao, L. Strongly Interacting C_{60}/Ir(111) Interface: Transformation of C_{60} into Graphene and Influence of Graphene Interlayer. *J. Phys. Chem. C* **2015**, *119*, 27550−27555.
(28) Pan, Y.; Zhang, H. G.; Shi, D. X.; Sun, J. T.; Du, S. X.; Liu, F.; Gao, H. J. Highly Ordered, Millimeter-Scale, Continuous, Single-Crystalline Graphene Monolayer Formed on Ru (0001). *Adv. Mater.* **2009**, *21*, 2777−2780.
(29) Sutter, P. W.; Flege, J.-I.; Sutter, E. A. Epitaxial Graphene on Ruthenium. *Nat. Mater.* **2008**, *7*, 406−411.
(30) Pan, L. D.; Que, Y. D.; Chen, H.; Wang, D. F.; Li, J.; Shen, C. M.; Xiao, W. D.; Du, S. X.; Gao, H. J.; Pantelides, S. T. Room-Temperature, Low-Barrier Boron Doping of Graphene. *Nano Lett.* **2015**, *15*, 6464−6468.
(31) Yu, Y. X. Can All Nitrogen-Doped Defects Improve the Performance of Graphene Anode Materials for Lithium-Ion Batteries? *Phys. Chem. Chem. Phys.* **2013**, *15*, 16819−16827.
(32) Li, X. L.; Wang, H. L.; Robinson, J. T.; Sanchez, H.; Diankov, G.; Dai, H. J. Simultaneous Nitrogen Doping and Reduction of Graphene Oxide. *J. Am. Chem. Soc.* **2009**, *131*, 15939−15944.
(33) Shao, Y. Y.; Zhang, S.; Engelhard, M. H.; Li, G. S.; Shao, G. C.; Wang, Y.; Liu, J.; Aksay, I. A.; Lin, Y. H. Nitrogen-Doped Graphene and Its Electrochemical Applications. *J. Mater. Chem.* **2010**, *20*, 7491−7496.
(34) Sheng, Z. H.; Shao, L.; Chen, J. J.; Bao, W. J.; Wang, F. B.; Xia, X. H. Catalyst-Free Synthesis of Nitrogen-Doped Graphene via Thermal Annealing Graphite Oxide with Melamine and Its Excellent Electrocatalysis. *ACS Nano* **2011**, *5*, 4350−4358.
(35) Miao, Q. H.; Wang, L. D.; Liu, Z. Y.; Wei, B.; Xu, F. B.; Fei, W. D. Magnetic Properties of N-Doped Graphene with High Curie Temperature. *Sci. Rep.* **2016**, *6*, 21832.
(36) Viswanathan, B.; Krishanmurthy, K. R. Nitrogen Incorporation in TiO_2: Does It Make a Visible Light Photo-Active Material? *Int. J. Photoenergy* **2012**, *2012*, 269654.
(37) Joucken, F.; Tison, Y.; Le Fèvre, P.; Tejeda, A.; Taleb-Ibrahimi, A.; Conrad, E.; Repain, V.; Chacon, C.; Bellec, A.; Girard, Y.; et al. Charge Transfer and Electronic Doping in Nitrogen-Doped Graphene. *Sci. Rep.* **2015**, *5*, 14564.
(38) Schiros, T.; Nordlund, D.; Palova, L.; Prezzi, D.; Zhao, L. Y.; Kim, K. S.; Wurstbauer, U.; Gutierrez, C.; Delongchamp, D.; Jaye, C.; et al. Connecting Dopant Bond Type with Electronic Structure in N-Doped Graphene. *Nano Lett.* **2012**, *12*, 4025−4031.
(39) Marchini, S.; Günther, S.; Wintterlin, J. Scanning Tunneling Microscopy of Graphene on Ru(0001). *Phys. Rev. B: Condens. Matter Mater. Phys.* **2007**, *76*, 075429.
(40) Preobrajenski, A. B.; Ng, M. L.; Vinogradov, A. S.; Mårtensson, N. Controlling Graphene Corrugation on Lattice-Mismatched Substrates. *Phys. Rev. B: Condens. Matter Mater. Phys.* **2008**, *78*, 073401.
(41) Luo, Z. Q.; Lim, S.; Tian, Z. Q.; Shang, J. Z.; Lai, L. F.; MacDonald, B.; Fu, C.; Shen, Z. X.; Yu, T.; Lin, J. Y. Pyridinic N Doped Graphene: Synthesis, Electronic Structure, and Electrocatalytic Property. *J. Mater. Chem.* **2011**, *21*, 8038−8044.
(42) Li, J. Y.; Li, X. H.; Zhao, P. H.; Lei, D. Y.; Li, W. L.; Bai, J. T.; Ren, Z. Y.; Xu, X. L. Searching for Magnetism in Pyrrolic N-Doped Graphene Synthesized via Hydrothermal Reaction. *Carbon* **2015**, *84*, 460−468.
(43) Navarro, J. J.; Leret, S.; Calleja, F.; Stradi, D.; Black, A.; Bernardo-Gavito, R.; Garnica, M.; Granados, D.; Vázquez de Parga, A. L.; Pérez, E. M.; et al. Organic Covalent Patterning of Nanostructured Graphene with Selectivity at the Atomic Level. *Nano Lett.* **2016**, *16*, 355−361.

DOI: 10.1021/acs.nanolett.7b00038
Nano Lett. 2017, 17, 2887−2894

(44) Kattel, S.; Atanassov, P.; Kiefer, B. Stability, Electronic and Magnetic Properties of In-Plane Defects in Graphene: A First-Principles Study. *J. Phys. Chem. C* **2012**, *116*, 8161−8166.
(45) Banhart, F.; Kotakoski, J.; Krasheninnikov, A. V. Structural Defects in Graphene. *ACS Nano* **2011**, *5*, 26−41.
(46) Guo, J. J.; Lee, J.; Contescu, C. I.; Gallego, N. C.; Pantelides, S. T.; Pennycook, S. J.; Moyer, B. A.; Chisholm, M. F. Crown Ethers in Graphene. *Nat. Commun.* **2014**, *5*, 5389.
(47) Rutter, G. M.; Crain, J. N.; Guisinger, N. P.; Li, T.; First, P. N.; Stroscio, J. A. Scattering and Interference in Epitaxial Graphene. *Science* **2007**, *317*, 219−222.
(48) Joucken, F.; Tison, Y.; Lagoute, J.; Dumont, J.; Cabosart, D.; Zheng, B.; Repain, V.; Chacon, C.; Girard, Y.; Botello-Méndez, A. R.; et al. Localized State and Charge Transfer in Nitrogen-Doped Graphene. *Phys. Rev. B: Condens. Matter Mater. Phys.* **2012**, *85*, 161408.
(49) Tison, Y.; Lagoute, J.; Repain, V.; Chacon, C.; Girard, Y.; Rousset, S.; Joucken, F.; Sharma, D.; Henrard, L.; Amara, H.; et al. Electronic Interaction between Nitrogen Atoms in Doped Graphene. *ACS Nano* **2015**, *9*, 670−678.
(50) Gao, L. Probing Electronic Properties of Graphene on the Atomic Scale by Scanning Tunneling Microscopy and Spectroscopy. *Graphene 2D Mater.* **2014**, *1*, 23−46.
(51) Giovannetti, G.; Khomyakov, P. A.; Brocks, G.; Karpan, V. M.; van den Brink, J.; Kelly, P. J. Doping Graphene with Metal Contacts. *Phys. Rev. Lett.* **2008**, *101*, 026803.
(52) Khomyakov, P. A.; Giovannetti, G.; Rusu, P. C.; Brocks, G.; van den Brink, J.; Kelly, P. J. First-Principles Study of the Interaction and Charge Transfer between Graphene and Metals. *Phys. Rev. B: Condens. Matter Mater. Phys.* **2009**, *79*, 195425.

DOI: 10.1021/acs.nanolett.7b00038
Nano Lett. 2017, 17, 2887−2894